Adsorptive Removal of Heavy Metals from Wastewater Using Bamboo and Coconut Biochar: A Modelling Approach

Manaswee Ipsita, Somesh Jena, Sunil Kumar, Narayan Chandra Moharana

Abstract: *Heavy metal persistence in aquatic systems continues to threaten ecological stability and public health, particularly where centralized treatment is limited. In this context, adsorption using waste derived carbon materials offers a technically viable and circular approach. This study evaluates coconut shell and bamboo derived biochar as low-cost adsorbents for copper (Cu^{2+}) and lead (Pb^{2+}) removal linking surface functionality with adsorption performance. Biochar was synthesized via slow pyrolysis and characterized for morphology, porosity, surface charge and functional groups that govern metal binding. Batch experiments assessed the effects of pH, dosage, contact time and initial concentration. Adsorption was strongly pH-dependent, with optimal uptake at pH 5-7. Rapid kinetics were observed, with equilibrium achieved at 60 min for Cu^{2+} and 45 min for Pb^{2+}. Isotherm analysis indicated distinct mechanisms. Cu^{2+} adsorption onto coconut shell biochar followed the Langmuir model (q_{max} = 102.67 mg/g, R^2 = 0.99), achieving 99.32% removal and suggesting monolayer coverage. In contrast, Pb^{2+} adsorption onto bamboo biochar followed the Freundlich model (n = 3.29, R^2 = 0.981) with 98.92% removal, indicating heterogeneous multilayer adsorption. Kinetics for both metals conformed to the pseudo-second-order model, implying chemisorption-dominated interactions. FTIR and zeta potential analyses confirmed the role of oxygen containing functional groups and surface charge in metal uptake. Beyond performance, this biochar integrates waste valorisation with water treatment, supporting low-energy, decentralized applications. Their effectiveness, coupled with feedstock-driven surface variability, underscores the need for a systems-oriented approach that considers adsorption efficiency alongside material lifecycle and environmental sustainability*

Manaswee Ipsita, National Institute of Technology- Rourkela, Sector 1, Rourkela – 769008, India
Somesh Jena, National Institute of Technology- Rourkela, Sector 1, Rourkela – 769008, India
Sunil Kumar (s_kumar@neeri.res.in), CSIR- National Environmental Engineering Research Institute (NEERI), Nehru Marg, Nagpur – 440020, India
Narayan Chandra Moharana, Kalinga Institute of Technology, Patia, Bhubaneswar – 751024, India

ISSN: 0262-8104 (print) 1756-3488 (online)

Keywords: Adsorption, Heavy metals, Isotherms, Kinetics, Sustainable wastewater treatment

Introduction

Heavy metal contamination in surface and subsurface waters, particularly from wastewater and leachate streams remains a major environmental and public health concern. Cu^{2+} and Pb^{2+} are among the most prevalent contaminants released from industrial activities such as mining, metal plating, battery manufacturing and wastewater discharge (Hama Aziz et al., 2023). Unlike organic pollutants, heavy metals are non-degradable and persist in the environment through bioaccumulation and biomagnification. Elevated Cu concentrations disrupt cellular functions and may lead to hepatic and renal impairment, gastrointestinal disorders, and neurological dysfunction (Taylor et al., 2020). Pb is highly toxic even at low exposure levels and affects the nervous system, kidney function, and cardiovascular health, with irreversible impacts, especially in children (Balali-Mood et al., 2021). These risks highlight the need for efficient and scalable remediation strategies. Conventional heavy metal removal technologies, including ion exchange, chemical precipitation, membrane filtration and electrocoagulation are widely applied but face practical limitations. High operational cost, energy demand and secondary waste generation often restrict their large-scale implementation, particularly at low metal concentrations. In contrast, sorption-based approaches provide a more economical and adaptable alternative. Biochar derived from agricultural residues are especially promising as they integrate waste valorisation with water treatment. Coconut biochar (CBC) obtained from carbon-rich coconut shells, typically exhibits a microporous structure and abundant functional groups that support metal uptake. Bamboo biochar (BBC) similarly presents a porous structure with reactive surface chemistry offering strong adsorption potential. Both materials are renewable, low-cost and reduce reliance on conventional treatments that generate secondary sludge or toxic by-products. Biochar is produced through pyrolysis under oxygen limited conditions, commonly within the range of 400-600°C and is known to enhance cation exchange capacity and surface reactivity. Adsorption performance depends strongly on operational conditions. A dosage range of 0.3-1.0 g/L is often reported as effective for maintaining adsorption efficiency(Zhao et al., 2019). Metal removal, particularly for Cu^{2+} and Pb^{2+} is typically enhanced at pH 5 to 7 due to reduced competition from H^{+} ions (Huang et al., 2017). Equilibrium is frequently reached within 5-60 minutes, and adsorption kinetics are commonly described by the pseudo-second-order model, indicating chemisorption-controlled interactions (Adabi et al., 2023; Zaimee et al., 2021).These trends reflect the coupled influence of surface charge, functional groups and solution chemistry. Despite extensive research, several challenges remain. Comparative studies evaluating coconut and bamboo derived biochar for Cu^{2+} and Pb^{2+} removal are limited. The combined effects of surface chemistry, porosity, pyrolysis conditions and functional group distribution on adsorption efficiency are not yet fully resolved. Key operational variables, including pH, adsorbent dosage, contact time and initial

metal concentration also require systematic optimization (David, 2022; Hama Aziz et al., 2023). In addition, adsorption mechanisms involving ion exchange, surface complexation, electrostatic interaction and precipitation need clearer interpretation to support material design and targeted applications (Zhao et al., 2019).

This work investigates the effectiveness of the reduction of Cu^{2+} and Pb^{2+} from liquid phase system with the aid of bamboo and coconut-based biochar, which could have advantages over existing remediation approaches. The primary intent of this research is to analyse the uptake efficiency of BBC and CBC in removing Cu^{2+} and Pb^{2+} ions from water samples through a comprehensive experimental approach. This study aims to (1) synthesize and characterize biochar from bamboo and coconut shells under controlled pyrolysis conditions, assessing their surface morphology, porosity, and functional groups (2) evaluate adsorption efficiency by examining the intervention of key parameters such as solution acidity, adsorbent quantity, exposure time and starting metal concentration (3) model adsorption rate equations based on site availability and chemisorption, including first and second models and those for heterogeneous adsorption energy. Equilibrium is examined using isotherms describing monolayer coverage, surface heterogeneity, and energy distribution (4) to elucidate the adsorption pathways governing Cu^{2+} and Pb^{2+} sequestration on biochar surfaces, with emphasis on the ion exchange, roles of surface complexation and electrostatic interactions in controlling metal removal.

Methodology

Biochar preparation

Selection and pre-treatment of raw materials

Bamboo and coconut cover were selected as biomass feedstock due to their high lignocellulosic content, rapid carbonization behaviour and enhanced surface reactivity. Sufficient raw materials were collected and hand-sorted to remove excess debris. They were then rinsed with deionized water to eliminate surface pollutants, particulate matter, and organic contaminants. The feedstocks were then air dried for 48h post washing and subsequently oven dried at 105°C for 24h to facilitate the removal of adsorbed moisture (Gai et al., 2014)(Castilla-Caballero et al., 2019).

Pyrolysis process

The pyrolysis of bamboo and coconut cover was conducted in a high temperature programmable Pyrolyzer under oxygen-limited conditions to control the thermochemical decomposition. The pyrolysis input parameters were optimized through literature review to achieve the desired properties. The BBC and CBC were obtained through pyrolysis conducted with a controlled temperature rise rate of 10°C/min, reaching a ultimate temperature of 600°C for a 2h holding period to facilitate complete thermal degradation.

High purity nitrogen was continuously circulated at a 150 mL/min flow rate to determine and maintain a non-reactive atmosphere, effectively inhibiting oxidation and secondary reactions. After the pyrolysis workflow biochar samples were naturally cooled in the pyrolyzer under continuous nitrogen flow to prevent oxidation and maintain structural integrity. The resulting biochar was then collected, ground up and screened resulting in a consistent particle size distribution of 0.5-1mm in accordance with ASTM standards. Fig.1 provides a schematic depiction of the pyrolysis apparatus used in this research.

Figure 1 Schematic illustration of the pyrolysis setup

Biochar characterization

A detailed physicochemical characterization of CBC and BBC was performed to elucidate the surface properties governing adsorption behaviour, including morphology, functional group distribution, porosity, elemental composition and electrokinetic response. These attributes define the active interface controlling metal uptake and stability under varying solution conditions. Surface morphology and structural integrity were examined using Scanning Electron Microscopy (SEM) (JEOL JSM-6480 LV, equipped with Energy Dispersive X-ray Spectroscopy, EDS). This analysis enabled visualization of surface texture, pore development and structural changes before and after metal adsorption, providing insight into adsorption induced morphological transformations. The chemical functionality of the biochar surface was analysed using Fourier Transform Infrared Spectroscopy (FTIR) (BRUKER VERTEX 70). Characteristic absorption bands corresponding to hydroxyl (-OH), carboxyl (-COOH), carbonyl (-C=O) and aromatic structures were identified, confirming the presence of oxygen containing functional groups. These groups play a critical role in metal binding, primarily through surface complexation and electrostatic interactions at the solid

solution interface. Textural properties were quantified using Brunauer Emmett Teller (BET) analysis (NOVA-touch 4 LX). Nitrogen adsorption desorption isotherms measured at 77.35 K were used to determine specific surface area, pore volume and pore size distribution. Pore morphology was further analysed using the Barrett Joyner Halenda (BJH) model providing a detailed understanding of mesoporous structure relevant to adsorption performance. Elemental compositions including carbon (C), hydrogen (H), nitrogen (N) and sulphur (S) was determined using a LECO CHNS analyser (628 series), offering insight into carbonization degree and chemical composition. Electrokinetic behaviour was assessed through zeta potential analysis (Malvern Zeta Sizer Nano ZS90) where surface charge was measured across varying pH conditions. This enabled evaluation of pH dependent surface charge dynamics and their influence on electrostatic interactions during metal adsorption(Zhou et al., 2022)(Guo et al., 2020).

Experiments for Batch adsorption

Batch adsorption tests were conducted to evaluate the removal of Pb^{2+} and Cu^{2+} ions from water using BBC and CBC. A stock solution (1L) of 1000mg/L of both metal ions was formulated, and dilute concentrations were subsequently formulated by dilution. The study was structured into three main sections: 1) The effect of biochar dosage was examined at 1g/L, 2g/L, 4g/L, 8g/L, 10g/L, 20g/L to 50 mL of Pb and Cu working solutions. The samples were agitated under magnetic agitation for 5h at 300rpm at ambient temperature. The biochar was removed by centrifuged from the adsorbate solutions at 550rpm for 5 min. samples were subsequently passed through Whatman Grade 42 filter paper, followed by further clarification using a 0.20 µm syringe filter to remove residual particulates. 2) The influence of solution acidity affecting metal adsorption was investigated at pH of 2, 3, 5, 7, 9 for both metals. The pH was regulated with the help of 0.1N NaOH and HCl solutions. 3) Adsorption isotherms analysis was performed varying starting concentrations of 10mg/L, 30mg/L, 50mg/L, 70mg/L, 100mg/L. Adsorption kinetics were analysed by evaluating the adsorption process at varying temporal stages of 15, 30, 45, 60, and 90 min.
The concentration after treatment of Pb and Cu was quantified by ICP-OES (Inductively Coupled Plasma Optical Emission Spectrometer, Thermo Fisher iCAP6300 DUO) and all measurements were done in triplicate to ensure reliability and accuracy (Su et al., 2022). The adsorption uptake and adsorption efficiency of both the ions by BBC and CBC were evaluated according to Eq.1 and Eq. 2.

$$qe = (Ci - Cf) \times \frac{V}{W} \qquad \text{…. (Eq.1)}$$

$$\text{Removal \%} = \frac{(Ci - Cf)}{Ci} \times 100 \qquad \text{…. (Eq.2)}$$

Given that,
q_e (mg/g) Indicates Cu^{2+} or Pb^{2+} adsorbed per biochar unit mass.
C_i (mg/L) and C_f (mg/L) denote the starting and final Cu^{2+} and Pb^{2+} concentrations in the solution, respectively.

W(g) mass of the biochar adsorbent (BBC and CBC) used in the study.
V (L) defined as the solvent volume containing metal ions.

Adsorption isotherms studies

In this research, the Langmuir, Freundlich, Dubinin-Radushkevich and Temkin adsorption isotherms have been implemented for calculating the adsorption data of Pb and Cu ions on the biochar examined under optimal pH at different dosages, initial concentrations and contact times (Kalam et al., 2021)(Elmorsi et al., 2014).

The Langmuir isotherm model (Eq. 3) was executed out to evaluate the monolayer binding potential of biochar for Cu^{2+} and Pb^{2+}.

$$qe = \frac{Qmax\ b\ Ce}{1+b\ Ce} \quad \text{… (Eq.3)}$$

Qmax represents the maximum adsorption capacity (mg/g)
b the Langmuir constant
Ce the equilibrium concentration (mg/L).
Determined from the slope and intercept of the *Ce*/*qe* vs *Ce* plot.

The separation factor (*RL*), derived from the Langmuir isotherm, assesses adsorption feasibility and favourability is expressed as Eq. 4.

$$RL = \frac{1}{(1+b\ Ce)} \quad \text{…. (Eq.4)}$$

The adsorption behaviour is categorized based on the RL value as follows:
RL > 1 Unfavourable adsorption, indicating weak sorption interaction.
RL = 1 Linear adsorption, suggesting a constant partitioning between the adsorbent and solution.
0 < *RL* < 1 Favourable adsorption, demonstrating efficient metal uptake onto the biochar surface.
RL = 0 Irreversible adsorption, where the metal ions exhibit permanent binding to the adsorbent (Al-Ghouti & Da'ana, 2020).
The Freundlich isotherm (Eqs.5 and 6) models' adsorption on heterogeneous surfaces, assuming multilayer adsorption with sites of unequal binding strengths.

$$qe = KFCe^{1/2} \quad \text{.... (Eq.5)}$$

$$\log qe = \log k + (\frac{1}{n}\log Ce) \quad \text{….(Eq.6)}$$

given that:
K*F* (L/g) Freundlich capacity constant, reflecting the capacity to adsorb.
n is the Freundlich intensity parameter, reflecting adsorption favourability and surface heterogeneity.
The value of 1/n provides insights into the adsorption characteristics:
1/*n* < 1 Favourable adsorption, strong adsorbate-adsorbent interactions.

$1/n = 1$ Linear adsorption, suggesting homogeneous surface binding.
$1/n > 1$ Unfavourable adsorption, indicating weak sorption interactions.
The Temkin isotherm considers adsorbate–adsorbent interactions and assumes that the heat of adsorption declines uniformly as surface coverage. Temkin isotherm model can be formulated as Eq. 7.

$$qe = B \ln \mathrm{KT} + B \ln Ce \quad \text{….(Eq.7)}$$

The linear form of Temkin's isotherm is stated as Eq. 8.

$$qe = \frac{\mathrm{RT}}{\mathrm{C}} \ln KT + \frac{\mathrm{RT}}{\mathrm{C}} \ln Ce \quad \text{….(Eq.8)}$$

Given that:
K_T (L/g) Temkin isotherm binding constant.
B (J/mol) Adsorption heat coefficient, given by $B = \mathrm{RT/C}$.
R (8.314 J/mol. K) Universal gas constant.
T (K) Absolute temperature.
C (J /mol) Temkin adsorption energy constant.
Here, B determines if adsorption is physisorption (low B) or chemisorption (high B), useful for systems with strong adsorbate-adsorbent interactions.
Dubinin-Radushkevich (D-R) isotherm exhibits adsorption on porous adsorbents by taking into account surface porosity and energy heterogeneity. Contrary to the Langmuir and Freundlich approaches, this particular system depends on Polanyi's potential theory, which describes adsorption as a pore-filling process driven by surface heterogeneity.
The mathematical representation of the D-R isotherm model is given by Eq. 9

$$qe = qm \exp(-k\mathcal{E}^2) \quad \text{…….(Eq.9)}$$

The linearized form of the D-R isotherm model is furnished as Eq. 10.

$$\ln qe = \ln qm - K\mathcal{E}^2 \quad \text{.....(Eq.10)}$$

Where:
q_m (mg/g) ultimate adsorption capacity.
K ($\mathrm{mol^2/KJ^2}$) adsorption energy constant indicating average adsorption free energy.
Ɛ Polanyi's potential.

$$\mathcal{E} = \mathrm{RT} \ln\left(1 + \frac{1}{Ce}\right) \quad \text{…..(Eq.11)}$$

The average adsorption enthalpy (E) is derived from K using Eq.12

$$\mathrm{E} = \frac{1}{\sqrt{2K}} \quad \text{…..(Eq. 12)}$$

If E < 8 KJ/mol, adsorption follows physisorption (non-covalent dispersive interactions).
If E > 8 KJ/mol, adsorption follows chemisorption (ion exchange or covalent bonding).
The model distinguishes between physisorption and chemisorption by analyzing the adsorption energy (E), providing insight into the dominant binding forces.

2.5 Adsorption rate kinetics

Metal ion adsorption kinetics determine the pace and interaction dynamics between sorbent and sorbate, which influences metal ion residence duration at the liquid-solid interface. (Li et al., 2007). This current research analysed the adsorption behaviour of Cu (II) and Pb (II) using BBC and CBC using pseudo-first-order (PFO), pseudo-second-order (PSO) and Elovich kinetic models.

The PFO kinetic model is mathematically represented as Eq.13.

$$\log(qe - qt) = \log qe - \mathrm{K1}\frac{t}{2.303} \quad \text{…. (Eq.13)}$$

Given that:
q_t (mg/g) adsorption capacity at a given time
K1(min^{-1}) rate constant of the PFO equation.
The PSO kinetic model is mathematically given by Eq.14

$$\frac{dq}{dt} = \mathrm{K2}(qe - q)^2 \quad \text{…. (Eq.14)}$$

Upon integration, the equation transforms into Eq.15

$$\frac{t}{qt} = \left(\frac{1}{\mathrm{k2}}qe^2\right) + \frac{t}{qe} \quad \text{…. (Eq.15)}$$

given that:

t (min) is the contact time.
K2 (g/mg·min) PSO rate constant.
These kinetics models are imperative for analyzing the adsorption mechanism and identifying whether the process follows physisorption (PFO) or chemisorption (PSO).
Elovich model describes chemisorption kinetics, assuming an exponential decrease in the adsorption rate as sites are occupied. It is particularly applicable to heterogeneous adsorption systems with non-uniform energy sites

Analytical expression of the Elovich Equation is formulated as Eq.16

$$qt = \frac{1}{\beta}\ln(\alpha\beta) + \frac{1}{\beta}\ln t \quad \text{…..(Eq.16)}$$

given that:
α (mg/g·min) Initial adsorption rate, describing the rate at which adsorption begins when $t \rightarrow 0$. A higher α suggests rapid initial adsorption.
β(g/mg) Desorption constant, linked to activation energy and surface coverage, defines the rate at which adsorption slows as sites become occupied.
ln Natural logarithm (base e) represents the logarithmic relationship between adsorption and time.

Results and discussion

Biochar Characterization

The morphological characteristics of the biochar as revealed by SEM analysis are presented in Fig. 2 (A & B). CBC exhibits a fragmented and highly porous surface marked by interconnected voids and cavity networks. This structure reflects the development of a stable carbon matrix with a high density of accessible adsorption sites. In contrast, BBC shows a more organized and aligned morphology with elongated, channel like pores consistent with the intrinsic vascular structure of bamboo. The relatively clean surface and well defined pore walls suggest efficient thermal decomposition with limited ash deposition. Overall, the distinct yet well-developed porous architectures of both CBC and BBC prior to adsorption indicate effective carbonization and structural preservation, which are critical for enhancing surface reactivity and adsorption performance (Z. Liu et al., 2024; Zeghioud et al., 2022). The surface functional chemistry of the biochar was further examined using FTIR, as illustrated in Fig. 2 (C & D). The spectra reveal the presence of key functional groups that govern adsorption behaviour. For CBC, characteristic peaks were observed at 3752.941 cm^{-1} corresponding to hydroxyl (-OH) groups, at 2343.638 cm^{-1} for carboxyl (C=O) functionalities, at 1455.540 cm^{-1} for C-O stretching, and at 1579.480 cm^{-1} associated with aliphatic (-CH) groups. Similarly, BBC exhibited peaks at 3688.740 cm^{-1} (-OH), 2343.638 cm^{-1} (C=O), 1449.794 cm^{-1} (C-O stretching), and 1658.509 cm^{-1} (aliphatic -CH)(Luo et al., 2024; Ray, 2020). These spectral features confirm the presence of oxygenated and aliphatic functional groups on both biochar. Such functionalities are central to adsorption, as they facilitate metal binding through surface complexation and electrostatic interactions, thereby enhancing the overall reactivity of the material (Bakshi et al., 2020).

(A) (B)

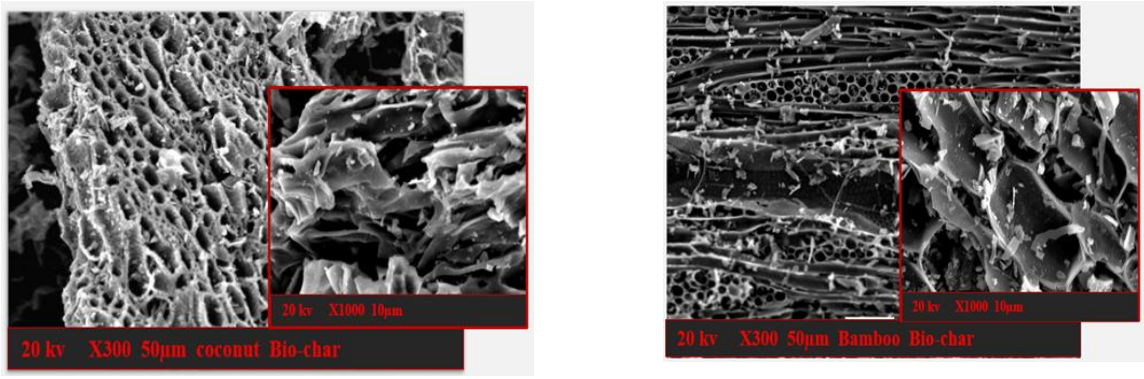

(C) (D)

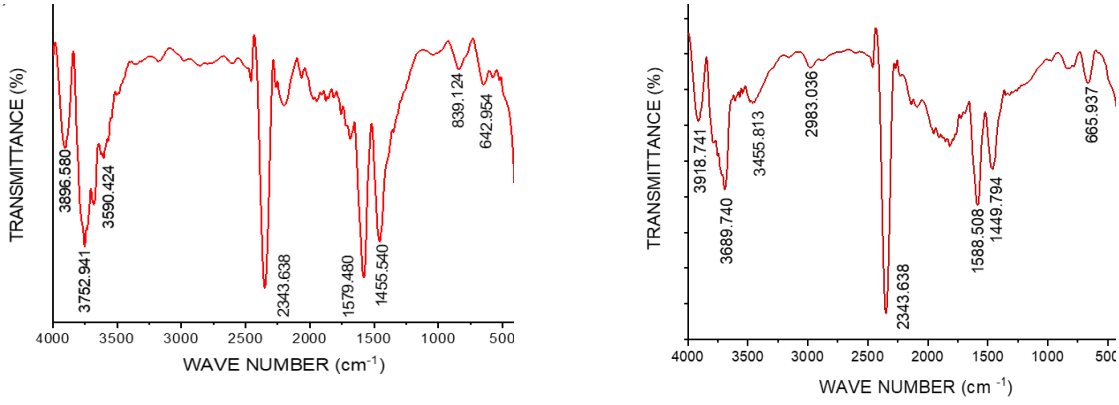

Figure 2 SEM micrographs of (A) CBC and (B) BBC, and the corresponding FTIR spectra of (C) CBC and (D) BBC.

The CHNS analysis (Table 1) indicates a high carbon content in both biochar, measured at 71.64 ± 0.05% for CBC and 73.82 ± 0.80% for BBC. This reflects a well-developed aromatic carbon framework which is favourable for adsorption processes. The hydrogen content was higher in CBC (3.55 ± 0.01%) compared to BBC (2.63 ± 0.08%), suggesting a relatively greater presence of surface hydroxyl (-OH) and carboxyl (-COOH) functionalities. Nitrogen

content remained consistent at 2.39% in both samples, while sulfur was minimal recorded at 0.05% for CBC and 0.04% for BBC, indicating only trace heteroatom incorporation from the biomass precursor. Oxygen content, estimated by difference was slightly higher in CBC implying a higher density of oxygenated functional groups. These compositional features collectively confirm the adsorption potential of both materials with CBC exhibiting a marginally higher surface reactivity due to enhanced functional group availability. The pore structure and surface characteristics were further evaluated using nitrogen adsorption desorption measurements at 77.35 K. BBC exhibited a specific surface area of 2.739 m^2/g ($r = 0.994$) with a BET constant (C) of 6.238 indicating moderate interaction between nitrogen molecules and the biochar surface.

The high correlation coefficient ($r = 0.994$) reflects a strong agreement between experimental data and BET theory supporting the reliability of the analysis (Thommes et al., 2015). The corresponding BJH analysis revealed an average pore radius of 1.88 nm and a total pore volume of 0.004 cc/g, consistent with a mesoporous structure. The Type IV isotherm with a small hysteresis loop further suggests capillary condensation within mesopores, indicating a well-developed pore network (Rouquerol et al., 2013). In comparison, CBC exhibited a higher surface area of 3.97 m^2/g ($r = 0.994$) and a BET constant of 6.47. The similarly high correlation coefficient confirms the robustness of the model fit, while the slightly higher C value suggests stronger nitrogen–surface interaction relative to BBC. This may indicate a more favourable adsorption environment. BJH analysis showed a mesopore volume of 0.004 cc/g and a peak pore radius of 3.8 nm further supporting the presence of mesoporous structures. Taken together, these results indicate that both biochar possess accessible pore networks, with CBC showing comparatively enhanced surface functionality and interaction potential, which may contribute to improved adsorption performance. The Type IV isotherm and narrow pore size range (1.6-3.9nm) confirm mesoporosity. Both biochar exhibit mesoporous structures, with BBC showing lower surface area and pore volume than CBC. Despite this, their mesopore distribution supports efficient heavy metal adsorption via surface metal ion interactions. (Ahmad et al., 2014). This suggests that their surface chemistry plays a pivotal role in metal ion sequestration, demonstrating potential for practical applications in environmental remediation (Inyang et al., 2016).

The electro kinetic attributes of BBC and CBC were investigated using zeta potential measurements over a wide range of pH to determine their surface charge characteristics. The results are included in Fig.3. A systematic decrease of zeta potential with an increase in pH was observed for both biochar samples, indicative of increased electrostatic repulsion at higher pH. The CBC sample consistently showed a higher zeta potential than the BBC sample across all the pH ranges indicating enhanced colloidal stability and unique surface chemical characteristics (Kamble et al., 2022; Rasmussen et al., 2020). Both samples exhibited a negative zeta potential at all pH ranges, with CBC beginning at -15 mV and BBC beginning at -20 mV. With an increase in pH up to 12, the zeta potential decreased to -40 mV for CBC and -45 mV for BBC. The isoelectric point of the biochar (pHIEP) was determined to be approximately pH 3.5, indicative of the change from a positively charged surface under highly acidic conditions to a negative surface under neutral to alkaline conditions(Liu et al.,

2016; Tran et al., 2018). A strong charge inversion was evident, due to the zeta potential changing from -4.73 mV (at pH 1.0) to -10.17 mV (at pH 2). This change indicates the enhanced electrostatic interaction with cationic metal ions by the biochar, thus favouring adsorption (Duwiejuah et al., 2020a; Ge et al., 2024). The negative surface potential observed above the pHIEP reduces electrostatic repulsion and enhances ion-exchange processes, thereby improving adsorption efficiency for heavy metals ions such as Cu^{2+} and Pb^{2+}. Further comparative analysis of zeta potential proved that CBC had a higher surface potential across all the ranges, indicating a unique functional group distribution that may enhance its potential for metal adsorption.

Table 1 Physicochemical characterization of CBC and BBC

Characteristics, Units	**Biochar**	**Biochar**
	Coconut cover Biochar	**Bamboo Biochar**
BET Surface area, m2/g	3.97 m²/g	2.739 m²/g
BJH Surface area(Pore-Surface Area)	2.43 m²/g	2.0063 m²/g
Average Pore Radius (BJH)	1.89 nm	1.88 nm
Pore Size Range	1.6-3.9 nm	1.5-2.5 nm
Fixed Solids (%)	2.56±0.39	1.90±0.02
Ash Content, (%)	6.69±0.17	9.04±0.34
pH	9.39±0.10	9.05±0.10
C, %	71.64±0.05	73.82±0.80
H, %	3.55±0.01	2.63±0.08
N, %	2.39±0.01	2.39±0.11
S, %	0.05±0.01	0.04±0.01
O, %	15.68	12.08

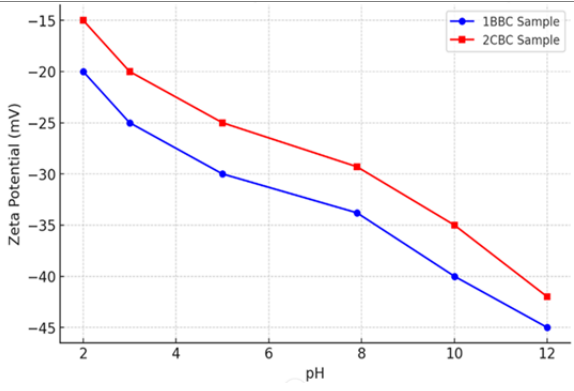

Figure 3 pH-Dependent Zeta Potential of BBC and CBC.

Impact of Operating Conditions on Batch Adsorption

Effect of Solution Acidity

The effect of solution pH on Cu^{2+} and Pb^{2+} adsorption is illustrated in Fig. 3, where acidity acts as a key regulator of adsorption through its influence on surface charge and metal speciation. At strongly acidic conditions (pH 1.0-3.0) adsorption is markedly suppressed due to competition from H^{+} ions, which protonate biochar functional groups and weaken electrostatic attraction. Even within this constraint, Pb^{2+} exhibits relatively higher uptake achieving removal efficiencies of 52.631% (CBC) and 57.353% (BBC), compared to 23.916% (CBC) and 26.656% (BBC) for Cu^{2+}. As the pH increases to 3.0-5.5 deprotonation of surface sites enhances metal binding leading to a sharp rise in adsorption efficiency(Q. Wang et al., 2018) At pH 3, Cu^{2+} removal improves to 80.123% (CBC) and 74.637% (BBC), while Pb^{2+} reaches 92.667% and 95.508% respectively. This regime reflects the growing contribution of ion exchange alongside electrostatic attraction. In the near-neutral range (pH 5.5-7.5) adsorption stabilizes at 98-99%, indicating near complete removal. At pH 7, Cu^{2+} removal reaches 98.965% (CBC) and 97.787% (BBC), while Pb^{2+} achieves 99.808% (CBC) and 98.997% (BBC). Here, adsorption is governed by strong electrostatic interactions coupled with surface complexation, enabled by the increasing density of negatively charged functional groups. Beyond pH 7.5 removal efficiencies remain high but the governing mechanism begins to shift. At pH 9, Pb^{2+} removal stabilizes at 99.327% (CBC) and 98.052% (BBC), while Cu^{2+} maintains 98.921% (CBC) and 98.367% (BBC). This apparent consistency is partly attributed to the formation of metal hydroxides such as $Cu(OH)_2$ and $Pb(OH)_2$, leading to flocculation rather than true adsorption (Babel & Kurniawan, 2003; Gupta & Ali, 2004; S. Wang & Peng, 2010).

Zeta potential analysis supports this transition, showing that increasing pH enhances the negative surface charge of biochar, thereby strengthening electrostatic attraction toward metal cations (Padilla et al., 2024). However, at extremely high pH, excess OH^{-} ions facilitate metal hydroxide precipitation, limiting further adsorption (Xu et al., 2022a). Overall, optimal adsorption occurs within the pH range of 3.0-7.5, where electrostatic interactions and surface complexation dominate (Afolabi & Musonge, 2023). Beyond pH 9, precipitation becomes significant, underscoring the need for precise pH control in optimizing biochar performance for heavy metal removal.

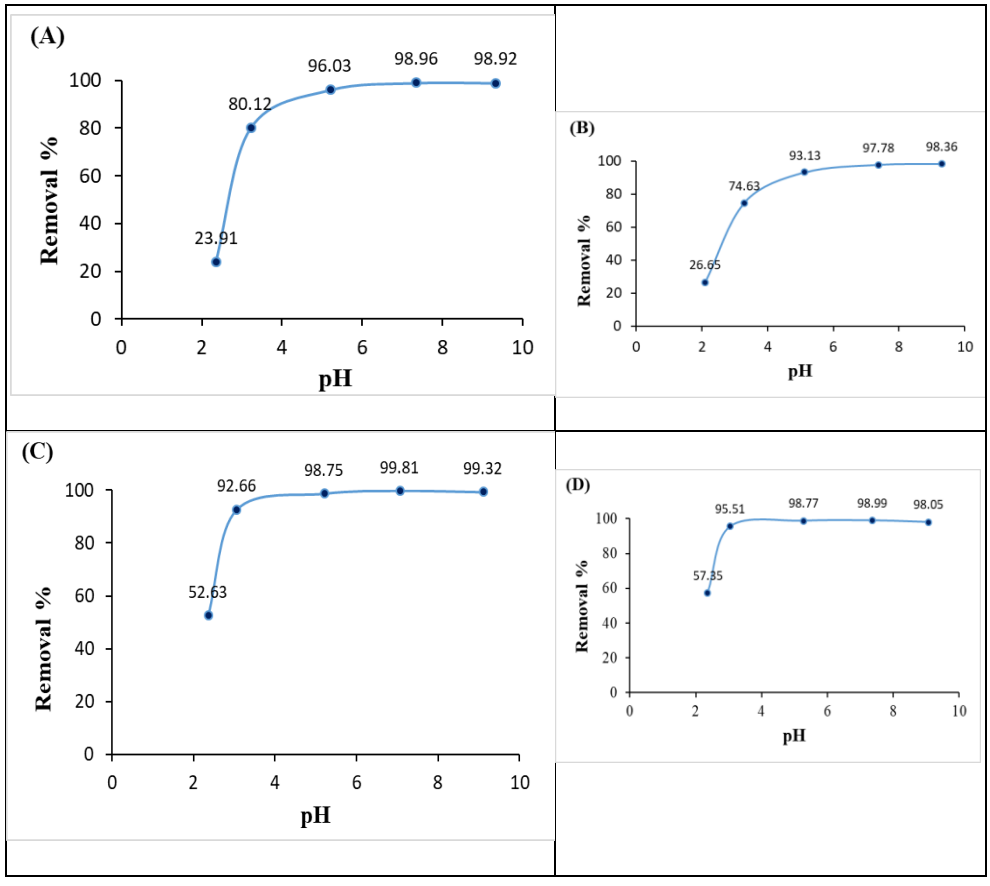

Figure 4 Effect of pH Variation on Adsorption Efficiency of (A) Cu2+ by CBC, (B) Cu2+ by BBC, (C) Pb2+ by CBC, and (D) Pb2+ by BBC. [Conditions: contact time = 3 hours; adsorbent dose = 0.08 g; solution volume = 50 mL

Effect of the adsorbent quantity

The influence of biochar dosage on the adsorption efficiency of Cu^{2+} and Pb^{2+} is presented in Fig. 5 (A, B), where a clear dosage-dependent enhancement is observed up to an optimal threshold. As the adsorbent concentration increases, the removal efficiency rises due to the progressive availability of active binding sites and an expanded effective surface area. However, beyond this optimum, the system approaches a saturation regime, where efficiency stabilizes or slightly declines due to particle aggregation, steric hindrance and mass transfer limitations (Chaudhary et al., 2024a).

For Cu^{2+}, the removal efficiency increases from 17.185% (CBC) and 19.311% (BBC) at a dosage of 1 g/L to 97.637% (CBC) and 95.159% (BBC) at 20 g/L. It can be ascribed to the

rise in available active binding sites and a higher adsorption surface area, which allows for metal ion capture(Bashir et al., 2022; Wilson et al., 2024).

A similar trend is observed for Pb^{2+} with removal efficiency rising from 27.551% (CBC) and 24.928% (BBC) at 1 g/L to 99.079% (CBC) and 96.45% (BBC) at 20 g/L. Notably, Pb^{2+} consistently demonstrates higher adsorption affinity compared to Cu^{2+}, which can be attributed to stronger electrostatic interactions and more stable binding with surface functional groups. This enhanced affinity persists even at shorter contact times and higher initial concentrations, indicating a preferential interaction pathway for Pb^{2+} on biochar surfaces (Jedaih et al., 2024). At concentrations exceeding the optimal level (i.e., 10 g/L for Pb^{2+}), adsorption efficiency plateaus as excess adsorbent causes aggregation, limiting surface accessibility and reducing active site availability (Wu et al., 2019; Xu et al., 2022b). Excessively applied biochar also causes resistance to diffusion and mass transfer, hindering metal effective adsorption. Hence, higher doses of biochar enhance metal removal through the additional provision of adsorption sites, but beyond the point of equilibrium in adsorbent-to-solute ratio, decreasing adsorption efficiency per unit mass occurs, pointing to the necessity of the right adsorbent dosage for optimum adsorption performance.

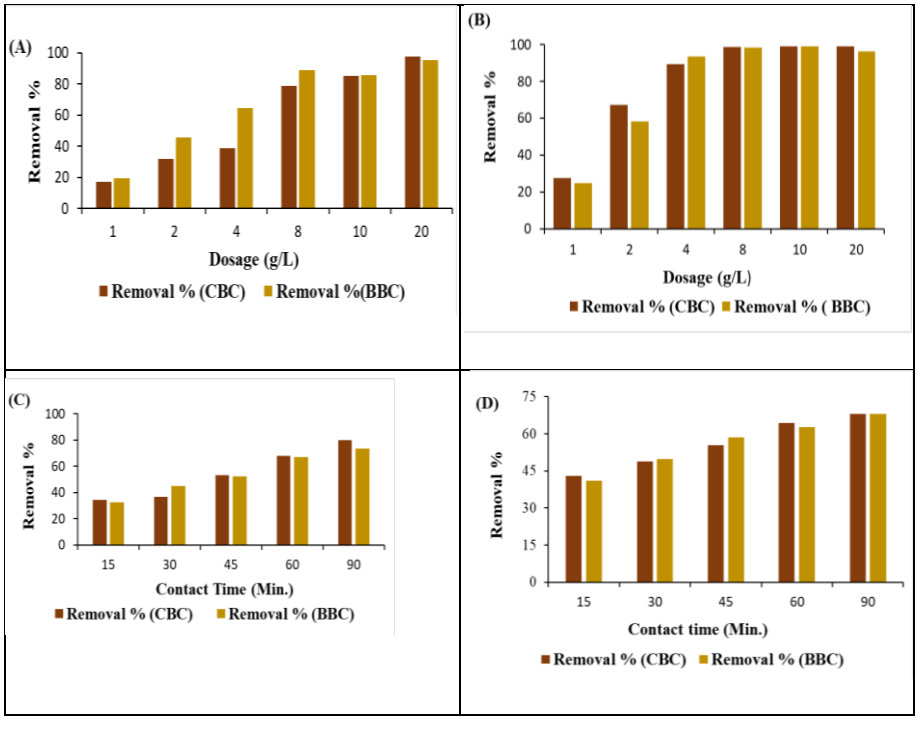

Figure 5 Effect of biochar dosage on the removal efficiencies of (A) Cu^{2+} by CBC and BBC (B) Pb^{2+} by CBC and BBC; Effect of contact time on the removal efficiencies of (C) Cu^{2+} by BBC and CBC, (D) Pb^{2+} by BBC and CBC [initial pH 5.5, adsorbent dosages 15g/L-90g/L, contact times 15 min - 90min].

Effect of exposure time

The time-dependent remediation performance of $Cu^{2+}$and Pb^{2+} by CBC and BBC were systematically examined to establish the equilibrium time and evaluate removal percentages; the corresponding results are illustrated in Fig.5(C, D). The percentage removal across varying contact durations from 15 to 90 min gives insights into the adsorption phenomena. The adsorption behaviour of Cu^{2+} was biphasic, with a quick initial phase within the first 60 minutes, followed by sluggish movement towards equilibrium. For CBC, the removal rate was 34.21% at 15 min, increased to 68.08% at 60 min, and reached 79.97% at 90 min. For BBC, the same trend was observed with a removal rate of 32.34% at 15 min, which increased to 67.22% at 60 min and reached the maximum of 73.74% at 90 min. The rapid initial rate of adsorption is driven by the presence of easily accessible active sites for binding, and the slow phase demonstrates a pore diffusion-controlled process due to overloading of the adsorption areas. (Duwiejuah et al., 2020b; Zhao et al., 2019). Pb^{2+} adsorption also followed a rapid initial phase, with 43.04% removal (CBC) and 41.09% (BBC) within the first 15 min. The removal continued with improving efficiency gradually, with 68.09% in CBC and 68.01% in BBC at 90 min, indicating that equilibrium was almost reached. Higher initial Pb^{2+} removal indicates stronger biochar affinity, driven by greater electrostatic attraction and coordination with surface groups. Adsorption of Pb^{2+} and Cu^{2+} by CBC and BBC are time-dependent and achieved equilibrium at approximately 90 min. On average, both the biochar exhibit efficient removal of heavy metals in a relatively short time.

Effect of starting metals concentration

The initial metal ion concentration plays a defining role in regulating adsorption performance as it governs the balance between solute availability in the aqueous phase and the finite number of active sites on the biochar surface. The corresponding behaviour is illustrated in Fig.6. At lower to moderate concentrations, sufficient active sites are available to accommodate incoming ions enabling efficient uptake. However, as concentration increases, this balance shifts toward site limitation and transport constraints. For Cu^{2+}, the optimum removal efficiency is observed at 80 mg/L, where CBC and BBC achieve 80.56% and 74.69%, respectively. Beyond this point, a decline in efficiency becomes evident, reaching 51.78% (CBC) and 28.92% (BBC) at 230 mg/L. This reduction is primarily associated with progressive saturation of active sites and increasing mass transfer resistance, which limits the diffusion of metal ions into the internal pore structure (Ahmad et al., 2012). A similar trend is noted for Pb^{2+}, with peak removal occurring at 55 mg/L, where efficiencies of 71.83% (CBC) and 70.56% (BBC) are achieved. Notably, Pb^{2+} demonstrates a consistently higher adsorption affinity compared to Cu^{2+}. This behaviour can be linked to its larger ionic radius and stronger electrostatic interactions, which facilitate more effective pore occupation and stable binding with surface functional groups. At elevated concentrations, the decline in removal efficiency for both metals reflects rapid site saturation, competitive ion interactions, and partial pore blocking, all of which restrict intra-particle diffusion and reduce overall

adsorption capacity (Wu et al., 2021; Zhan et al., 2023). Despite these constraints, the observed adsorption capacities at 79.971 mg/L for Cu^{2+} and 76.108 mg/L for Pb^{2+} highlight the governing role of biochar physicochemical properties in controlling metal sequestration. These findings reinforce the potential of biochar as an effective adsorbent for wastewater remediation (Lee et al., 2017). At higher loading conditions, however, system performance becomes increasingly limited by saturation effects. This suggests that material modification strategies or staged adsorption approaches may be required to sustain efficiency, particularly in concentrated waste streams, aligning adsorption design with resource recovery and circular treatment frameworks. In high-concentration systems, however, biochar modification or sequential adsorption processes may be inevitable to circumvent saturation effects and optimize overall performance.

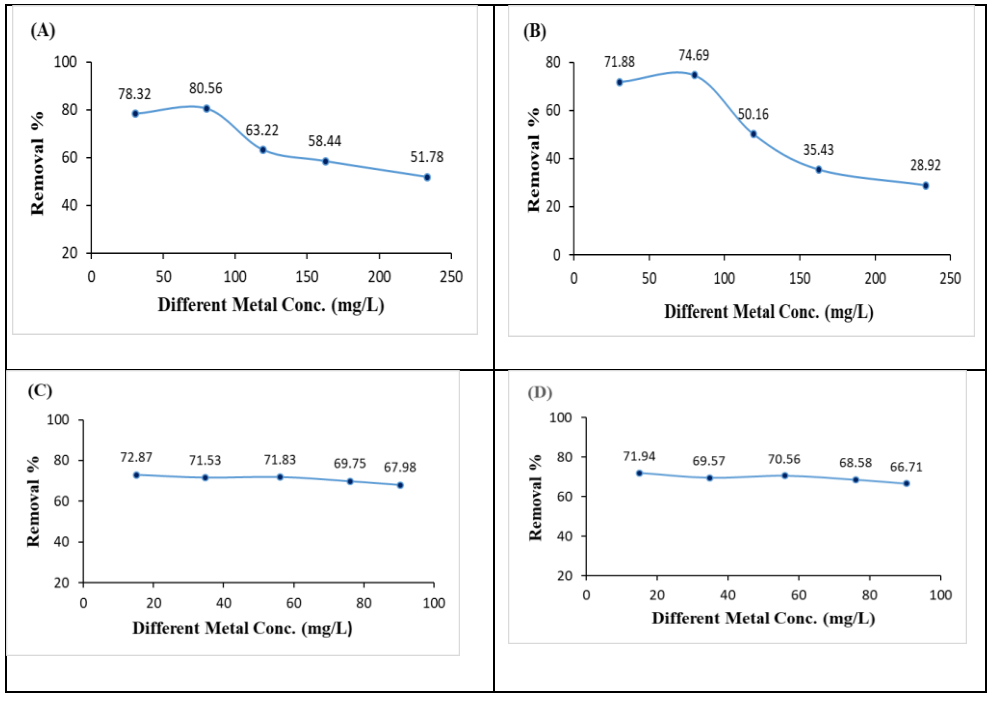

Figure 6 *Effect of starting metal concentration on Cu^{2+} and Pb^{2+} removal by CBC and BBC. (A) Cu^{2+} removal with CBC, (B) $Cu2^{+}$ removal with BBC, (C) Pb^{2+} removal with CBC, and (D) Pb^{2+} removal with BBC. [Conditions: contact time = 60min (Cu^{2+}) and 45min(Pb^{2+}); adsorbent dose = 0.08 g; solution volume = 50 mL.]*

Adsorption Modelling

Isotherm Fitting

The adsorption behaviour of Cu^{2+} and Pb^{2+} onto the CBC and BBC were evaluated through Langmuir, Freundlich, D-R and Temkin isotherm models. The analysis highlights distinct variations in adsorption capacity, process favourability, and model conformity across the two biochar. The results of Langmuir model for Pb^{2+} adsorption Provided evidence that, the q max values were 182.15 mg/g for CBC and 160 mg/g for BBC, with very high correlation coefficients R^2 =0.999 for CBC and R^2=0.998 for BBC). Cu^{2+} also recorded qmax values of 102.67 mg/g for CBC and 53.19 mg/g for BBC, and the corresponding R^2 values of 0.954 and 0.874, respectively. The RL, which is a measure of favourability ($0 < RL < 1$ is favourable adsorption), was between 0.13 and 1.87, and this indicated favourable adsorption conditions for all the concentrations tested. The Freundlich isotherm model for Cu^{2+} adsorption on CBC, indicated that KF was 7.03 mg/g and n was 1.947 which indicates favourable adsorption conditions ($1<n<10$). For BBC, KF was greater at 9.81 mg/g, with n=3.293, indicating greater binding affinity owing to greater surface heterogeneity of biochar from biological materials. Pb^{2+} also had greater KF values of 7.03 mg/g for CBC and 9.81 mg/g for BBC, with n values between 1.95 and 3.29, indicating efficient multilayer adsorption mechanisms. The Temkin model captures adsorbate–adsorbent interactions by accounting for the progressive decrease in adsorption enthalpy with increasing surface coverage, reflecting lateral interactions between adsorbed species. Within this framework, Cu^{2+} adsorption shows a clear distinction between the two biochar. The Temkin constant (B_t) for CBC is 132.27 J/mol, whereas BBC exhibits a significantly higher value of 336.80 J/mol, indicating stronger adsorbate–adsorbent interactions in BBC under comparable conditions. In contrast, Pb^{2+} adsorption yields nearly identical B_t values for CBC (156.83 J/mol) and BBC (155.10 J/mol), suggesting comparable interaction intensities across both surfaces.

The D-R model further resolves the nature of adsorption through the mean free energy (E), where values below 8 kJ/mol indicate physisorption and those in the range of 8–16 kJ/mol suggest chemisorption. For Cu^{2+} adsorption on CBC, the calculated E is 70.3 kJ/mol, clearly indicating a chemisorption-dominated mechanism. This interaction is further intensified in BBC, where E increases to 91.4 kJ/mol, reflecting stronger chemical affinity between Cu^{2+} ions and the biochar surface. A more pronounced trend is observed for Pb^{2+} adsorption. The E values for CBC and BBC are 2,420 kJ/mol and 2,460 kJ/mol, respectively, indicating an overwhelmingly chemisorption-controlled process. These substantially higher energy values, relative to Cu^{2+}, suggest stronger binding interactions, likely involving stable surface complexation and possible inner-sphere coordination. Taken together, the Temkin and D-R analyses converge on a consistent interpretation: while both biochar support chemisorption-driven uptake, BBC exhibits relatively stronger interaction intensity for Cu^{2+}, whereas Pb^{2+} adsorption is uniformly dominated by high-energy binding across both materials. This distinction reflects how surface energetics, shaped by biomass origin and carbonization pathways, govern not only adsorption capacity but also interaction stability an aspect central

to long-term performance, regeneration potential, and material circularity in adsorption systems.

Table 2 Equilibrium Isotherm Data for Cu^{2+} and Pb^{2+} on CBC and BBC Biochar.

Isotherms	**Parameters**	**Cu^{2+} CBC**	**Cu^{2+} BBC**	**Pb^{2+} CBC**	**Pb^{2+} BBC**
Langmuir	Qmax, mg/g	102.669	53.191	182.149	160
	R_L	0.548-0.136	0.425-0.087	1.145-1.870	1.156-1.941
	R^2	0.954	0.874	0.999	0.998
Freundlich	n_F	1.947	3.293	1.120	1.118
	$K_{F,}$ L/g	7.029	9.806	2.009	1.883
	R^2	0.893	0.635	0.996	0.995
Temkin	$A_{t,}$ L/mg	0.369	1.865	0.327	0.299
	$b_{t,}$ KJ/mol	132.273	336.806	156.836	155.105
	R^2	0.945	0.662	0.964	0.956
Dubinin-Radushkevich	qm, mol/g	0.0325	282.381	2.346	1.831
	K, $(mol\ KJ^{-1})^2$	1.01E-04	5.99E-05	2.07E-04	2.03E-04
	E, KJ/mol	7.03E+01	9.15E+01	2.42E+03	2.46+03
	R^2	0.893	0.635	0.986	0.986

Kinetic Fitting

The adsorption behaviour of Cu^{2+} and Pb^{2+} on CBC and BBC was evaluated by applying the PFO, PSO, and Elovich kinetic models to the experimental data. Table 3 presents the corresponding model factors and correlation coefficients. The adsorption rate constants (k_1, k_2), correlation coefficients (R^2) and equilibrium adsorption capacities (q_e) were determined to elucidate the underlying mechanisms of metal ion adsorption (Lim et al., 2019) (Zhang et al., 2023).

PFO adsorption kinetics were evaluated using the linearized Lagergren equation, in which $\ln(q_e-q_t)$ versus t plots allowed the determination of k_1 (Revellame et al., 2020). The R^2 of Cu^{2+} adsorption on CBC (0.832) and BBC (0.921) and Pb^{2+} adsorption on CBC (0.959) and BBC (0.993) indicated moderate to strong agreement with experimental data. However, significant deviations between calculated q_e were observed. Cu^{2+} adsorption q_e values were 100.39 mg/g for CBC and 68.43 mg/g for BBC, while Pb^{2+} adsorption reached 17.55 mg/g and 18.29 mg/g, respectively. These deviations indicate that physisorption alone cannot adequately describe the observed adsorption behaviour, pointing instead to more complex surface interactions (Askeland et al., 2020). To resolve this, the PSO kinetic model was applied by plotting t/q_t versus t, enabling the determination of the rate constant (k_2) and theoretical equilibrium adsorption capacity (q_e). The PSO model exhibited a strong agreement with the experimental data, reflected in higher correlation coefficients for Cu^{2+} adsorption onto CBC ($R^2 = 0.940$) and BBC ($R^2 = 0.964$), as well as for Pb^{2+} adsorption onto CBC ($R^2 = 0.985$) and BBC ($R^2 = 0.996$). In addition, the q_e values predicted by the model closely aligned with experimental observations, reinforcing its suitability in describing the system.

This strong model conformity indicates that chemisorption governs the adsorption process, involving electron sharing or exchange between the biochar surface and metal ions. A direct comparison across kinetic models further establishes the superiority of the PSO framework, as evidenced by both the higher R^2 values and the minimal deviation between calculated and experimental q_e values.

The Elovich kinetic model provides additional support for this interpretation, capturing the heterogeneity of surface energetics and the progressive nature of chemisorption. For Cu^{2+} adsorption, the model demonstrates strong agreement with experimental data, yielding R^2 values of 0.951 for CBC and 0.963 for BBC. The corresponding Elovich constants were $\alpha = 57.92$ and $\beta = 0.077$ for CBC, and $\alpha = 50.383$ and $\beta = 0.083$ for BBC, respectively. These parameters indicate favourable adsorption kinetics, with a high initial adsorption rate (α) followed by a gradual decrease governed by surface coverage and activation energy barriers. Taken together, the convergence of PSO and Elovich models highlights a chemisorption-dominated pathway, controlled by surface heterogeneity and active site interactions. This mechanistic clarity is critical for predicting adsorption performance under variable loading conditions and for designing biochar systems with sustained efficiency and regeneration potential.

Similarly, Pb^{2+} adsorption exhibited a strong fit to the Elovich model, with R^2 values of 0.949 for CBC and 0.991 for BBC. The corresponding Elovich parameters were determined as α = 5.541 mg/g·min and β = 0.192 g/mg for CBC, and α = 5.908 mg/g·min and β = 0.184 g/mg for BBC, reflecting consistent adsorption kinetics across both biochar. The comparatively higher β values obtained for Pb^{2+} indicate greater adsorption energy barriers, reflecting stronger and more stable interactions with the biochar surface, particularly in the case of BBC. This behaviour suggests a more energetically demanding yet stable chemisorption pathway for Pb^{2+} relative to Cu^{2+}. In this context, the Elovich model effectively complements the PSO results, collectively reaffirming the dominance of chemisorption while also indicating the comparatively superior adsorption performance of BBC.

A stringent comparison across kinetic models further substantiates the superiority of the PSO model over the PFO framework, as evidenced by higher correlation coefficients and negligible deviation between theoretical and experimental q_e values. The Elovich model similarly demonstrates strong conformity with experimental data, particularly for Pb^{2+} adsorption onto BBC (R^2 = 0.991) reinforcing the prevalence of chemisorption-controlled processes. Its ability to account for surface heterogeneity and variable activation energies provides an additional mechanistic layer, capturing the complexity of metal–biochar interactions beyond idealized assumptions. Taken together, these kinetic insights consistently indicate that the adsorption of Cu^{2+} and Pb^{2+} onto CBC and BBC is governed predominantly by chemisorption rather than diffusion-limited physisorption. The rate constant analysis further reveals a higher binding affinity of Pb^{2+} toward the biochar matrix, which can be attributed to its larger ionic radius and higher effective charge density, enabling stronger coordination with surface functional groups. As a result, Pb^{2+} exhibits consistently higher adsorption efficiency compared to Cu^{2+} under identical experimental conditions.

Overall, the convergence of PSO and Elovich models provides a robust and internally consistent description of the adsorption kinetics, confirming that chemisorption-driven mechanisms dominate metal sequestration. This mechanistic clarity not only strengthens predictive reliability but also highlights the role of surface chemistry and structural heterogeneity in governing selective adsorption behaviour in biochar-based system.

Table 2 Kinetic Model Parameters for Cu and Pb Adsorption onto CCB and BBC Biochar.

Heavy Metal	**Bio-char**	**Experimental qe (mg/g)**	**PFO K_1**	**qe (mg/g)**	**R^2**	**PSO K_2**	**qe (mg/g)**	**exp(R)**	**ELOVICH α**	**β**	**R^2**
Cu^{2+}	CBC	40.269	0.057	100.394	0.832	0.004	57.175	0.940	57.925	0.077	0.951
Cu^{2+}	BBC	37.332	0.051	68.432	0.920	0.005	51.175	0.964	50.383	0.083	0.963

Pb^{2+}	CBC	25.164	0.028	17.552	0.959	0.002	27.987	0.985	5.541	0.192	0.949
Pb^{2+}	BBC	24.718	0.032	18.286	0.993	0.002	27.847	0.996	5.908	0.184	0.991

Mechanism Governing Adsorption

Adsorption of Cu^{2+} and Pb^{2+} by CCB and BBC biochar is a complex surface-controlled process with surface complexation, ion exchange, electrostatic attraction, precipitation, and pore filling dominating the process (Murtaza et al., 2022). BET surface area analysis authenticated the refined porous matrix and high porosity of CCB and BBC biochar considerably enhanced the adsorption capacity by offering a high surface area and well-interconnected micropore architecture for immobilizing metal ions(Zhou et al., 2022). FTIR shifts confirm strong binding of Pb^{2+} and Cu^{2+} to biochar's hydroxyl (-OH), carboxyl (-COOH), and carbonyl (C=O) groups forming stable metal complexes. Reduction in intensity of such functional group bands after adsorption confirms that metal immobilization involves prevalent chemical bonding, hydrogen bonding, and coordination interactions. Zeta potential determination also confirmed the role of pH in adsorption effectiveness, wherein increasing the solution pH led to a more negative biochar surface charge, enhancing electrostatic attraction with cationic Pb^{2+} and Cu^{2+} species. This was most evident in the pH-dependent adsorption trend, wherein metal ion uptake was greater at more basic pH values due to greater dissociation of functional groups and more intense ion-exchange process(Petrović et al., 2016). SEM imaging also delivered useful information on the mechanism of adsorption by detecting extreme changes in the morphology of biochar following adsorption, such as metal ion deposition, surface agglomeration, and partial pore blocking, which indicate both surface and intraparticle diffusion-controlled adsorption (Mei et al., 2025) (Fahmi et al., 2018). Secondly, π-π electron donor acceptor interactions between aromatic moieties in the biochar matrix and metal ions likely contribute to the adsorption of Pb^{2+} and Cu^{2+} onto CBC and BBC. In addition, participation of oxygen-containing functional groups to facilitate chelation-like coordination interactions cannot be overlooked considering that the groups have been shown to enhance metal-binding selectivity and stability. Participation of mineral compounds in biochar could also influence metal adsorption through precipitation processes, hence enhancing removal efficiency. The synergistic effect of these mechanisms reflects that CCB and BBC biochar have notable adsorption efficiencies for Pb^{2+} and Cu^{2+}, thus making them extremely promising for low-cost and environment friendly methods of heavy metal removal. However, to enhance their practical application even more, future research must focus on long-term adsorption stability, render ability and competitive adsorption behaviour in real wastewater matrices (Amin et al., 2018) (Alsawy et al., 2022).

Conclusion

This study establishes CBC and BBC as effective, low cost and sustainable adsorbents for the removal of Cu^{2+} and Pb^{2+} from aqueous systems. Physicochemical characterization confirms the development of well-defined porous structures with appreciable surface area and the presence of key oxygenated functional groups (-OH, -COOH, -C=O) which actively participate in metal binding. Adsorption performance emerges from the coupled action of electrostatic attraction, surface complexation and ion exchange indicating a multi-mechanistic pathway governing metal sequestration. Isotherm modelling provides further resolution of these interactions. Cu^{2+} adsorption conforms predominantly to the Langmuir model suggesting monolayer coverage over energetically uniform sites whereas Pb^{2+} adsorption aligns better with the Freundlich model, reflecting heterogeneous surface interactions and multilayer uptake. The calculated maximum adsorption capacities and favourable separation factor (RL) values consistently confirm the feasibility and efficiency of the adsorption process. The Temkin model indicates a progressive decrease in adsorption energy with increasing surface coverage, while comparatively stronger interaction parameters for BBC point to its enhanced adsorption potential. The D-R model further identifies chemisorption as the governing mechanism, driven by high-energy interactions between metal ions and functionalized biochar surfaces. Kinetic analysis reinforces this interpretation. The PSO model provides the best fit for both Cu^{2+} and Pb^{2+} adsorption, indicating that the rate-limiting step is governed by chemisorption involving electron sharing or exchange. The Elovich model further supports this mechanism, particularly for Pb^{2+} adsorption onto BBC ($R^2 = 0.991$) highlighting the role of heterogeneous surface energies and activated chemisorptive interactions. Intraparticle diffusion analysis suggests that while pore diffusion contributes to the overall process, it is not the sole rate controlling step confirming a hybrid mechanism involving both surface reaction and diffusion.

Overall, the findings demonstrate that bamboo and coconut derived biochar possess significant potential for heavy metal remediation, combining material efficiency with environmental compatibility. However, translation to real world systems requires further optimization of operational parameters such as pH, adsorbent dosage, contact time and initial metal concentration. Future work should focus on competitive adsorption in multi-component systems, regeneration and reuse strategies and pilot scale validation using real wastewater streams. In addition, targeted surface modification approaches may further enhance selectivity and adsorption capacity. Addressing these aspects will be critical for advancing biochar-based adsorption systems toward scalable, circular and application-ready water treatment solutions.

Collectively, this work advances a mechanistically grounded understanding of biochar-mediated heavy metal sequestration, positioning lignocellulosic waste-derived biochar as scalable, high-efficiency materials for next-generation water treatment systems.

Acknowledgements
The authors acknowledge the Council of Scientific and Industrial Research (CSIR), CSIR-HRDG, New Delhi, India and its constituent laboratory CSIR- National Environmental Engineering Research Institute (NEERI), Nagpur, India, for supporting the research.

References

Hama Aziz, K. H., Mustafa, F. S., Omer, K. M., et al. (2023). Heavy metal pollution in the aquatic environment: Efficient and low-cost removal approaches to eliminate their toxicity: A review. *RSC Advances, 13*, 17595–17610.

Taylor, A. A., Tsuji, J. S., Garry, M. R., et al. (2020). Critical review of exposure and effects: Implications for setting regulatory health criteria for ingested copper. *Environmental Management, 65*, 131–159.

Balali-Mood, M., Naseri, K., Tahergorabi, Z., et al. (2021). Toxic mechanisms of five heavy metals: Mercury, lead, chromium, cadmium, and arsenic. *Frontiers in Pharmacology, 12*, 643972.

Zhao, J., Shen, X. J., Domene, X., et al. (2019). Comparison of biochar derived from different types of feedstock and their potential for heavy metal removal in multiple-metal solutions. *Scientific Reports, 9*, 9869.

Huang, J., Yuan, F., Zeng, G., et al. (2017). Influence of pH on heavy metal speciation and removal from wastewater using micellar-enhanced ultrafiltration. *Chemosphere, 173*, 199–206.

Adabi, S., Yazdanbakhsh, A., Shahsavani, A., et al. (2023). Removal of heavy metals from the aqueous solution by nanomaterials: A review with analyzing and categorizing the studies. *Journal of Environmental Health Science and Engineering, 21*, 305–318.

Zaimee, M. Z. A., Sarjadi, M. S., & Rahman, M. L. (2021). Heavy metals removal from water by efficient adsorbents. *Water, 13*, 2659.

David, E. (2022). Production of activated biochar derived from residual biomass for adsorption of volatile organic compounds. *Materials, 16*, 389.

A. O. D. (2012). Langmuir, Freundlich, Temkin and Dubinin–Radushkevich isotherms studies of equilibrium sorption of Zn^{2+} onto phosphoric acid modified rice husk. *IOSR Journal of Applied Chemistry, 3*, 38–45.

Kalam, S., Abu-Khamsin, S. A., Kamal, M. S., & Patil, S. (2021). Surfactant adsorption isotherms: A review. *ACS Omega, 6*, 32342–32348.

Al-Ghouti, M. A., & Da'ana, D. A. (2020). Guidelines for the use and interpretation of adsorption isotherm models: A review. *Journal of Hazardous Materials, 393*, 122383.

Li, Q., Zhai, J., Zhang, W., et al. (2007). Kinetic studies of adsorption of Pb(II), Cr(III) and Cu(II) from aqueous solution by sawdust and modified peanut husk. *Journal of Hazardous Materials, 141*, 163–167.

Liu, Z., Zhou, S., Cai, Y., et al. (2024). Mechanisms of chromium removal from water and soil using bioleached nano zero-valent iron-mediated biochar via co-pyrolysis. *Nanomaterials, 14*, 1895.

Zeghioud, H., Fryda, L., Mahieu, A., et al. (2022). Potential of flax shives and beech wood-derived biochar in methylene blue and carbamazepine removal from aqueous solutions. Materials, 15, 2824.

Luo, Q., Deng, Y., Li, Y., et al. (2024). Effects of pyrolysis temperatures on the structural properties of straw biochar and its adsorption of tris-(1-chloro-2-propyl) phosphate. Scientific Reports, 14, 25711.

Ray, A. (2020). Characterization of biochar from various agricultural by-products using FTIR spectroscopy, SEM focused with image processing. International Journal of Agriculture, Environment and Biotechnology, 13.

Bakshi, S., Banik, C., & Laird, D. A. (2020). Estimating the organic oxygen content of biochar. Scientific Reports, 10, 13082.

Brunauer, S., Emmett, P. H., & Teller, E. (1938). Adsorption of gases in multimolecular layers. Journal of the American Chemical Society, 60, 309–319.

Thommes, M., Kaneko, K., Neimark, A. V., et al. (2015). Physisorption of gases, with special reference to the evaluation of surface area and pore size distribution. Pure and Applied Chemistry, 87, 1051–1069.

Rouquerol, J., Rouquerol, F., Llewellyn, P., et al. (2013). Adsorption by powders and porous solids: Principles, methodology and applications. Academic Press.

Sing, K. S. W. (1985). Reporting physisorption data for gas/solid systems with special reference to the determination of surface area and porosity. Pure and Applied Chemistry, 57, 603–619.

Ahmad, M., Rajapaksha, A. U., Lim, J. E., et al. (2014). Biochar as a sorbent for contaminant management in soil and water: A review. Chemosphere, 99, 19–33.

Inyang, M. I., Gao, B., Yao, Y., et al. (2016). A review of biochar as a low-cost adsorbent for aqueous heavy metal removal. Critical Reviews in Environmental Science and Technology, 46, 406–433.

Kamble, S., Agrawal, S., Cherumukkil, S., et al. (2022). Revisiting zeta potential, the key feature of interfacial phenomena, with applications and recent advancements. ChemistrySelect, 7, e202103084.

Rasmussen, M. K., Pedersen, J. N., & Marie, R. (2020). Size and surface charge characterization of nanoparticles with a salt gradient. Nature Communications, 11, 2337.

Adabi, S., Yazdanbakhsh, A., Shahsavani, A., Sheikhmohammadi, A., & Hadi, M. (2023). Removal of heavy metals from the aqueous solution by nanomaterials: A review with analysing and categorizing the studies. Journal of Environmental Health Science and Engineering, 21(2), 305–318. https://doi.org/10.1007/s40201-023-00863-0

Afolabi, F. O., & Musonge, P. (2023). Synthesis, Characterization, and Biosorption of Cu2+ and Pb2+ Ions from an Aqueous Solution Using Biochar Derived from Orange Peels. Molecules, 28(20), 7050. https://doi.org/10.3390/molecules28207050

Ahmad, M., Lee, S. S., Dou, X., Mohan, D., Sung, J.-K., Yang, J. E., & Ok, Y. S. (2012). Effects of pyrolysis temperature on soybean stover- and peanut shell-derived biochar properties and TCE adsorption in water. Bioresource Technology, 118, 536–544. https://doi.org/10.1016/j.biortech.2012.05.042

Ahmad, M., Rajapaksha, A. U., Lim, J. E., Zhang, M., Bolan, N., Mohan, D., Vithanage, M., Lee, S. S., & Ok, Y. S. (2014). Biochar as a sorbent for contaminant management in soil and water: A review. Chemosphere, 99, 19–33. https://doi.org/10.1016/j.chemosphere.2013.10.071

Al-Ghouti, M. A., & Da'ana, D. A. (2020). Guidelines for the use and interpretation of adsorption isotherm models: A review. Journal of Hazardous Materials, 393, 122383. https://doi.org/10.1016/j.jhazmat.2020.122383

Alsawy, T., Rashad, E., El-Qelish, M., & Mohammed, R. H. (2022). A comprehensive review on the chemical regeneration of biochar adsorbent for sustainable wastewater treatment. Npj Clean Water, 5(1), 29. https://doi.org/10.1038/s41545-022-00172-3

Amin, M. T., Alazba, A. A., & Shafiq, M. (2018). Removal of Copper and Lead using Banana Biochar in Batch Adsorption Systems: Isotherms and Kinetic Studies. Arabian Journal for Science and Engineering, 43(11), 5711–5722. https://doi.org/10.1007/s13369-017-2934-z

A.O, D. (2012). Langmuir, Freundlich, Temkin and Dubinin–Radushkevich Isotherms Studies of Equilibrium Sorption of Zn 2+ Unto Phosphoric Acid Modified Rice Husk. IOSR Journal of Applied Chemistry, 3(1), 38–45. https://doi.org/10.9790/5736-0313845

Askeland, M., Clarke, B. O., Cheema, S. A., Mendez, A., Gasco, G., & Paz-Ferreiro, J. (2020). Biochar sorption of PFOS, PFOA, PFHxS and PFHxA in two soils with contrasting texture. Chemosphere, 249, 126072. https://doi.org/10.1016/j.chemosphere.2020.126072

Babel, S., & Kurniawan, T. A. (2003). Low-cost adsorbents for heavy metals uptake from contaminated water: A review. Journal of Hazardous Materials, 97(1), 219–243. https://doi.org/10.1016/S0304-3894(02)00263-7

Bakshi, S., Banik, C., & Laird, D. A. (2020). Estimating the organic oxygen content of biochar. Scientific Reports, 10(1), 13082. https://doi.org/10.1038/s41598-020-69798-y

Balali-Mood, M., Naseri, K., Tahergorabi, Z., Khazdair, M. R., & Sadeghi, M. (2021). Toxic Mechanisms of Five Heavy Metals: Mercury, Lead, Chromium, Cadmium, and Arsenic. Frontiers in Pharmacology, 12, 643972. https://doi.org/10.3389/fphar.2021.643972

Bashir, M., Mohan, C., Tyagi, S., & Annachhatre, A. (2022). Copper removal from aqueous solution using chemical precipitation and adsorption by Himalayan Pine Forest Residue as Biochar. Water Science and Technology, 86(3), 530–554. https://doi.org/10.2166/wst.2022.222

Castilla-Caballero, D., Barraza-Burgos, J., Gunasekaran, S., Roa-Espinosa, A., Colina-Márquez, J., Machuca-Martínez, F., Hernández-Ramírez, A., & Vázquez-Rodríguez, S. (2019). Experimental data on the production and characterization of biochar derived from coconut-shell wastes obtained from the Colombian Pacific Coast at low temperature pyrolysis. Data in Brief, 28, 104855. https://doi.org/10.1016/j.dib.2019.104855

Chaudhary, H., Dinakaran, J., Notup, T., Vikram, K., & Rao, K. S. (2024a). Comparison of Adsorption Performance of Biochar Derived from Urban Biowaste Materials for Removal of Heavy Metals. Environmental Management, 73(2), 408–424. https://doi.org/10.1007/s00267-023-01866-1

Chaudhary, H., Dinakaran, J., Notup, T., Vikram, K., & Rao, K. S. (2024b). Comparison of Adsorption Performance of Biochar Derived from Urban Biowaste Materials for Removal of Heavy Metals. Environmental Management, 73(2), 408–424. https://doi.org/10.1007/s00267-023-01866-1

David, E. (2022). Production of Activated Biochar Derived from Residual Biomass for Adsorption of Volatile Organic Compounds. Materials, 16(1), 389. https://doi.org/10.3390/ma16010389

Duwiejuah, A. B., Abubakari, A. H., Quainoo, A. K., & Amadu, Y. (2020a). Review of Biochar Properties and Remediation of Metal Pollution of Water and Soil. Journal of Health and Pollution, 10(27), 200902. https://doi.org/10.5696/2156-9614-10.27.200902

Duwiejuah, A. B., Abubakari, A. H., Quainoo, A. K., & Amadu, Y. (2020b). Review of Biochar Properties and Remediation of Metal Pollution of Water and Soil. Journal of Health & Pollution, 10(27), 200902. https://doi.org/10.5696/2156-9614-10.27.200902

Elmorsi, T. M., Mohamed, Z. H., Shopak, W., & Ismaiel, A. M. (2014). Kinetic and Equilibrium Isotherms Studies of Adsorption of Pb(II) from Water onto Natural Adsorbent.

Journal of Environmental Protection, 05(17), 1667–1681. https://doi.org/10.4236/jep.2014.517157

Fahmi, A. H., Samsuri, A. W., Jol, H., & Singh, D. (n.d.). Physical modification of biochar to expose the inner pores and their functional groups to enhance lead adsorption. RSC Advances, 8(67), 38270–38280. https://doi.org/10.1039/c8ra06867d

Gai, X., Wang, H., Liu, J., Zhai, L., Liu, S., Ren, T., & Liu, H. (2014). Effects of Feedstock and Pyrolysis Temperature on Biochar Adsorption of Ammonium and Nitrate. PLoS ONE, 9(12), e113888. https://doi.org/10.1371/journal.pone.0113888

Ge, S., Zhao, S., Wang, L., Zhao, Z., Wang, S., & Tian, C. (2024). Exploring adsorption capacity and mechanisms involved in cadmium removal from aqueous solutions by biochar derived from euhalophyte. Scientific Reports, 14(1), 450. https://doi.org/10.1038/s41598-023-50525-2

Guo, C., Zou, J., Yang, J., Wang, K., & Song, S. (2020). Surface characterization of maize-straw-derived biochar and their sorption mechanism for Pb2+ and methylene blue. PLoS ONE, 15(8), e0238105. https://doi.org/10.1371/journal.pone.0238105

Gupta, V. K., & Ali, I. (2004). Removal of lead and chromium from wastewater using bagasse fly ash—A sugar industry waste. Journal of Colloid and Interface Science, 271(2), 321–328. https://doi.org/10.1016/j.jcis.2003.11.007

Hama Aziz, K. H., Mustafa, F. S., Omer, K. M., Hama, S., Hamarawf, R. F., & Rahman, K. O. (2023). Heavy metal pollution in the aquatic environment: Efficient and low-cost removal approaches to eliminate their toxicity: a review. RSC Advances, 13(26), 17595–17610. https://doi.org/10.1039/d3ra00723e

Huang, J., Yuan, F., Zeng, G., Li, X., Gu, Y., Shi, L., Liu, W., & Shi, Y. (2017). Influence of pH on heavy metal speciation and removal from wastewater using micellar-enhanced ultrafiltration. Chemosphere, 173, 199–206. https://doi.org/10.1016/j.chemosphere.2016.12.137

Inyang, M. I., Gao ,Bin, Yao ,Ying, Xue ,Yingwen, Zimmerman ,Andrew, Mosa ,Ahmed, Pullammanappallil ,Pratap, Ok ,Yong Sik, & and Cao, X. (2016). A review of biochar as a low-cost adsorbent for aqueous heavy metal removal. Critical Reviews in Environmental Science and Technology, 46(4), 406–433. https://doi.org/10.1080/10643389.2015.1096880

Jedaih, M. A., Salem, Z. A., & Alzboon, K. (2024). Biochar for Lead Removal from Aqueous Solution.

Kalam, S., Abu-Khamsin, S. A., Kamal, M. S., & Patil, S. (2021). Surfactant Adsorption Isotherms: A Review. ACS Omega, 6(48), 32342–32348. https://doi.org/10.1021/acsomega.1c04661

Kamble, S., Agrawal, S., Cherumukkil, S., Sharma, V., Jasra, R. V., & Munshi, P. (2022). Revisiting Zeta Potential, the Key Feature of Interfacial Phenomena, with Applications and Recent Advancements. ChemistrySelect, 7(1), e202103084. https://doi.org/10.1002/slct.202103084

Lee, M.-E., Park, J. H., & Chung, J. W. (2017). Adsorption of Pb(II) and Cu(II) by Ginkgo-Leaf-Derived Biochar Produced under Various Carbonization Temperatures and Times. International Journal of Environmental Research and Public Health, 14(12), 1528. https://doi.org/10.3390/ijerph14121528

Li, Q., Zhai, J., Zhang, W., Wang, M., & Zhou, J. (2007). Kinetic studies of adsorption of Pb(II), Cr(III) and Cu(II) from aqueous solution by sawdust and modified peanut husk. Journal of Hazardous Materials, 141(1), 163–167. https://doi.org/10.1016/j.jhazmat.2006.06.109

Lim, W.-R., Kim, S. W., Lee, C.-H., Choi, E.-K., Oh, M. H., Seo, S. N., Park, H.-J., & Hamm, S.-Y. (2019). Performance of composite mineral adsorbents for removing Cu, Cd, and Pb ions from polluted water. Scientific Reports, 9, 13598. https://doi.org/10.1038/s41598-019-49857-9

Liu, C.-H., Chuang, Y.-H., Li, H., Teppen, B. J., Boyd, S. A., Gonzalez, J. M., Johnston, C. T., Lehmann, J., & Zhang, W. (2016). Sorption of Lincomycin by Manure-Derived Biochar from Water. Journal of Environmental Quality, 45(2), 519–527. https://doi.org/10.2134/jeq2015.06.0320

Liu, Z., Zhou, S., Cai, Y., Zhang, X., Shaaban, M., Peng, Q., & Cai, Y. (2024). Mechanisms of Chromium Removal from Water and Soil Using Bioleached Nano Zero-Valent Iron-Mediated Biochar via Co-Pyrolysis. Nanomaterials, 14(23), Article 23. https://doi.org/10.3390/nano14231895

Luo, Q., Deng, Y., Li, Y., He, Q., Wu, H., & Fang, X. (2024). Effects of pyrolysis temperatures on the structural properties of straw biochar and its adsorption of tris-(1-chloro-2-propyl) phosphate. Scientific Reports, 14(1), 25711. https://doi.org/10.1038/s41598-024-77299-5

Mei, Y., Zhuang, S., & Wang, J. (2025). Adsorption of heavy metals by biochar in aqueous solution: A review. Science of The Total Environment, 968, 178898. https://doi.org/10.1016/j.scitotenv.2025.178898

Padilla, J. T., Watts, D. W., Szogi, A. A., & Johnson, M. G. (2024). Evaluation of a pH- and time-dependent model for the sorption of heavy metal cations by poultry litter-derived biochar. Chemosphere, 347, 140688. https://doi.org/10.1016/j.chemosphere.2023.140688

Petrović, J., Lačnjevac, Č., & Stanković, S. (2016). Characterization and usefulness of corn cob as biosorbent for Pb2+, Cu2+ and Zn2+ ions removal from aqueous solutions. Zastita Materijala, 57(3), 480–487. https://doi.org/10.5937/ZasMat1603480P

Rasmussen, M. K., Pedersen, J. N., & Marie, R. (2020). Size and surface charge characterization of nanoparticles with a salt gradient. Nature Communications, 11(1), 2337. https://doi.org/10.1038/s41467-020-15889-3

Ray, A. (2020). Characterization of Biochar from Various Agricultural By-Products Using FTIR Spectroscopy, SEM focused with image Processing. International Journal of Agriculture Environment and Biotechnology, 13(4). https://doi.org/10.30954/0974-1712.04.2020.6

Revellame, E. D., Fortela, D. L., Sharp, W., Hernandez, R., & Zappi, M. E. (2020). Adsorption kinetic modeling using pseudo-first order and pseudo-second order rate laws: A review. Cleaner Engineering and Technology, 1, 100032. https://doi.org/10.1016/j.clet.2020.100032

Rouquerol, J., Rouquerol, F., Llewellyn, P., Maurin, G., & Sing, K. (2013). Adsorption by Powders and Porous Solids: Principles, Methodology and Applications. Academic Press.

Su, X., Chen, Y., Li, Y., Li, J., Song, W., Li, X., & Yan, L. (2022). Enhanced adsorption of aqueous Pb(II) and Cu(II) by biochar loaded with layered double hydroxide: Crucial role of mineral precipitation. Journal of Molecular Liquids, 357, 119083. https://doi.org/10.1016/j.molliq.2022.119083

Taylor, A. A., Tsuji, J. S., Garry, M. R., McArdle, M. E., Goodfellow, W. L., Adams, W. J., & Menzie, C. A. (2020). Critical Review of Exposure and Effects: Implications for Setting Regulatory Health Criteria for Ingested Copper. Environmental Management, 65(1), 131–159. https://doi.org/10.1007/s00267-019-01234-y

Thommes, M., Kaneko, K., Neimark, A. V., Olivier, J. P., Rodriguez-Reinoso, F., Rouquerol, J., & Sing, K. S. W. (2015). Physisorption of gases, with special reference to the evaluation of surface area and pore size distribution (IUPAC Technical Report). Pure and Applied Chemistry, 87(9–10), 1051–1069. https://doi.org/10.1515/pac-2014-1117

Tran, H. N., Lee ,Chung-Kung, Nguyen ,Tien Vinh, & and Chao, H.-P. (2018). Saccharide-derived microporous spherical biochar prepared from hydrothermal carbonization and different pyrolysis temperatures: Synthesis, characterization, and application in water treatment. Environmental Technology, 39(21), 2747–2760. https://doi.org/10.1080/09593330.2017.1365941

Wang, Q., Wang, B., Lee, X., Lehmann, J., & Gao, B. (2018). Sorption and desorption of Pb(II) to biochar as affected by oxidation and pH. Science of The Total Environment, 634, 188–194. https://doi.org/10.1016/j.scitotenv.2018.03.189

Wang, S., & Peng, Y. (2010). Natural zeolites as effective adsorbents in water and wastewater treatment. Chemical Engineering Journal, 156(1), 11–24. https://doi.org/10.1016/j.cej.2009.10.029

Wilson, K., Iqbal, J., Obaid Abdalla Obaid Hableel, A., Naji Khalaf Beyaha Alzaabi, Z., & Nazzal, Y. (2024). Camel Dung-Derived Biochar for the Removal of Copper(II) and Chromium(III) Ions from Aqueous Solutions: Adsorption and Kinetics Studies. ACS Omega, 9(10), 11500–11509. https://doi.org/10.1021/acsomega.3c08230

Wu, Q., Dong, S., Wang, L., & Li, X. (2021). Single and Competitive Adsorption Behaviors of Cu2+, Pb2+ and Zn2+ on the Biochar and Magnetic Biochar of Pomelo Peel in Aqueous Solution. Water, 13(6), Article 6. https://doi.org/10.3390/w13060868

Wu, Q., Xian, Y., He, Z., Zhang, Q., Wu, J., Yang, G., Zhang, X., Qi, H., Ma, J., Xiao, Y., & Long, L. (2019). Adsorption characteristics of Pb(II) using biochar derived from spent mushroom substrate. Scientific Reports, 9, 15999. https://doi.org/10.1038/s41598-019-52554-2

Xu, Y., Qu, Y., Yang, Y., Qu, B., Shan, R., Yuan, H., & Sun, Y. (2022a). Study on Efficient Adsorption Mechanism of Pb2+ by Magnetic Coconut Biochar. International Journal of Molecular Sciences, 23(22), 14053. https://doi.org/10.3390/ijms232214053

Xu, Y., Qu, Y., Yang, Y., Qu, B., Shan, R., Yuan, H., & Sun, Y. (2022b). Study on Efficient Adsorption Mechanism of Pb2+ by Magnetic Coconut Biochar. International Journal of Molecular Sciences, 23(22), 14053. https://doi.org/10.3390/ijms232214053

Ye, Q., Li, Q., & Li, X. (2022). Removal of heavy metals from wastewater using biochar: Adsorption and mechanisms. Environmental Pollutants and Bioavailability. (world). https://www.tandfonline.com/doi/abs/10.1080/26395940.2022.2120542

Zaimee, M. Z. A., Sarjadi, M. S., & Rahman, M. L. (2021). Heavy Metals Removal from Water by Efficient Adsorbents. Water, 13(19), Article 19. https://doi.org/10.3390/w13192659

Zeghioud, H., Fryda, L., Mahieu, A., Visser, R., & Kane, A. (2022). Potential of Flax Shives and Beech Wood-Derived Biochar in Methylene Blue and Carbamazepine Removal from Aqueous Solutions. Materials, 15(8), Article 8. https://doi.org/10.3390/ma15082824

Zhan, D., Ye, A., & Hou, T. (2023). Research progress on biochar-based material adsorption and removal of ibuprofen. Frontiers in Environmental Science, 11. https://doi.org/10.3389/fenvs.2023.1327000

Zhang, H., Zhong, W., Qiu, R., & Han, L. (2023). Kinetics and modeling of Pb (II) adsorption in pellet biochar based on micro-computed tomography characterization. Bioresource Technology, 387, 129645. https://doi.org/10.1016/j.biortech.2023.129645

Zhao, J., Shen, X.-J., Domene, X., Alcañiz, J.-M., Liao, X., & Palet, C. (2019). Comparison of biochar derived from different types of feedstock and their potential for heavy metal removal in multiple-metal solutions. Scientific Reports, 9, 9869. https://doi.org/10.1038/s41598-019-46234-4

Zhou, R., Zhang, M., & Shao, S. (2022). Optimization of target biochar for the adsorption of target heavy metal ion. Scientific Reports, 12(1), 13662. https://doi.org/10.1038/s41598-022-17901-w